Supplementary

Materials and Methods

Colorectal cancer cohort and tissue microarray slides

Tissue samples from stage III colorectal cancer (CRC) patients were obtained from Beaumont Hospital/RCSI, Dublin, Ireland, Queen's University Belfast, Northern Ireland, and Paris Descartes University, Paris, France. The de-identified samples were acquired per institutional guidelines. All centers provided ethical approval for this study, and informed consent was obtained from all participants. Six control cell lines were included in the tissue microarray (TMA) block along with 79 paraffin-embedded patient tumor core samples. The six control cell lines included in the TMA block were: HCT116 SMAC-KO; HCT116 XIAP-KO; JURKAT; HeLa; MCF7; and SKMEL Three TMA slides were generated from three consecutive 5-micron slices. Only four of the six control cell lines were of good quality and remained fixed to the slide throughout the staining and imaging process.

The TMA slides were baked, deparaffinized, and rehydrated followed by heat mediated antigen retrieval in citrate buffer (pH 6) and Tris EDTA buffer (pH 9) and blocked overnight in normal serum. All process steps were executed as a batch. After DAPI staining, slides were imaged using a Nikon 20x (0.75 NA) objective on an IN Cell 2200 (Cytiva, Issaquah, WA). Background imaging was performed across all relevant channels followed by antibody staining of two markers per round plus DAPI, dye deactivation, and repeat staining to collect 24 biomarkers labeled with either Cy3 or Cy5 (Supplementary Table S1) over 14 cycles (Supplementary Table S2). Staining was performed using an automated system (Leica Bond-MAX) to standardize antibody volumes, application, and incubation times. A DAPI re-charge was coupled to each staining and dye-inactivation step such that the signal was refreshed twice per cycle.

Each spot on the TMA slide was imaged at 20x magnification. Each field of view (FOV) image is 2560 x 2160 pixels^2 (998.4 x 842.4 microns^2). The pixel intensity value for image was stored as an unsigned 16-bit image file thus the intensity values ranged from 0 to 65,535 (or 2^{16}). The raw images underwent FOV illumination correction [described in US10746980B2]. Images from multiple rounds of staining and imaging underwent a registration step [described in US10088658B2]. The marker channels (but not the DAPI channel) underwent autofluorescence removal. The registered DAPI images for each of the 85 sample positions on the TMA slide were

segmented into nuclei objects (Vu 2019) implemented in python plugin for image J (described in Gerdes et al 2013). The segmentation algorithm utilizes specific stains to delineate cells and subcellular regions. DAPI staining is employed to segment nuclear area, Na+/K+-ATPase and pan-cadherin staining is used to segment cell membrane area, and pan-cytokeratin and/or E-cadherin antibody staining is used to segment epithelial from stromal regions. For more details see on segmentation see Gerdes et al (2013). A total of 297,430 nuclei objects were generated by segmenting the DAPI images from the first TMA slide A1.

Supplementary Table S1. List of twenty-four antibodies used in multiplexed analysis of the TMAs.

Target	Clone	Vendor	Catalog
APAF-1	2E12	Millipore	MAB3053
Bak	D4E4	Cell Signaling	12105
Bax	E63	Abcam	ab216985
BCL-2	124	Lifespan	LS-C389442
Bcl-xL	7D9	Thermo	MS-1334
CA9	polyclonal	Thermo	PA1-16592
Caspase-3 (Pro+cleaved)	D3R6Y	Cell Signaling	14214
Caspase-9	96.1.23	Santa Cruz	sc-56076 A647
CD3	F7.2.38	Dako	M7254
CD4	EPR6855	Abcam	ab181724
CD8	C8/144B	Dako	M7103
CD45	2B11 + PD7/26	Dako	M0701
Cytokeratin AE1	AE1	eBioscience	14-9001
Cytokeratin PCK26	PCK26	Sigma	C1801
FOXP3	206D	Biolegend	320014
Glut-1	EPR3915	Abcam	ab196357
HLA I	EMR8 5	Abcam	ab70328
Ki67	SP6	Zeta	Z2031
MCL-1	Y37	Abcam	ab186822
NAKATPase	EP1845Y	Abcam	ab167390
S6	C-8	Santa Cruz	sc-74459 A647
Smac	79-1-83	Cell Signaling	2954
PD1	EPR4877(2)	Abcam	ab201825
XIAP (API3)	polyclonal	Thermo	APH937

Supplementary Table S2. Rounds of staining for three TMA slides (A1, A2, and A3).

Round	Time between Rounds (Days)	Slide Order			Dapi round name	Dapi exposure time	Cy3 round name	Cy3 exposure time	Cy5 round name	Cy5 exposure time	Time between imaging slides (minutes)	
RG001		A1	A2	A3	bkgnd	50	bkgnd	400			6.1	27.0
RG002	1.2	A1	A2	A3	bkgnd	20	bkgnd	200	bkgnd	500	27.2	10.8
RG003	4.1	A3	A1	A2	dapi	20	BCL2	200	APAF1	1500	43.4	9.1
RG005	1.8	A1	A2	A3	dapi	20	MCL1	200	Casp9	1500	14.1	18.9
RG007	8.0	A2	A1	A3	dapi	50	S6a	400	Casp3	1500	9.9	39.1
RG008	4.9	A1	A2	A3	dapi	100	S6b	400			7.2	22.1
RG009	0.2	A2	A3	A1	bleach	100	bleach	200	bleach	500	32.9	38.4
RG010	0.8	A1	A2	A3	dapi	100	Bax	400	Smac	1500	78.3	16.2
RG011	1.0	A1	A2	A3	bleach	100	bleach	200	bleach	500	7.6	90.7
RG012	2.8	A1	A2	A3	dapi	100	Bak	400	XIAP	1500	9.7	28.2
RG013	0.8	A3	A1	A2	bleach	100	bleach	200	bleach	500	41.0	36.8
RG014	0.1	A1	A2	A3	dapi	100	NaKATPase	400	BCLXL	1500	18.6	17.8
RG015	1.1	A1	A2	A3	dapi	100	PCK26	100	CD8	1500	8.8	18.3
RG016	0.8	A1	A2	A3	bleach	100	bleach	200	bleach	500	7.5	17.4
RG017	0.1	A1	A2	A3	dapi	100	AE1	200	FOXP3	1500	9.6	20.6
RG018	1.0	A1		A3	dapi	100	CD4	200	Ki67	500	20.8	31.2
RG018	0.0		A2		dapi	50	CD4	200	Ki67	500	20.8	31.2
RG019	2.8	A1	A2	A3	bleach	100	bleach	200	bleach	500	7.9	9.8
RG020	0.2	A1	A2	A3	dapi	100	HLA_I	200	CD45	1500	10.1	85.6
RG021	0.9	A1	A2	A3	dapi	100	Glut1	400	CA9	1500	10.1	30.5
RG022	0.9	A1	A2	A3	dapi	100	CD3	400	PD1	1500	10.2	35.0
RG023	14.8	A1	A2	A3	bleach	50	bleach	200	bleach	500	9.2	92.8
RG024	0.1	A1	A2	A3	dapi	50			S6	1500	9.3	30.3

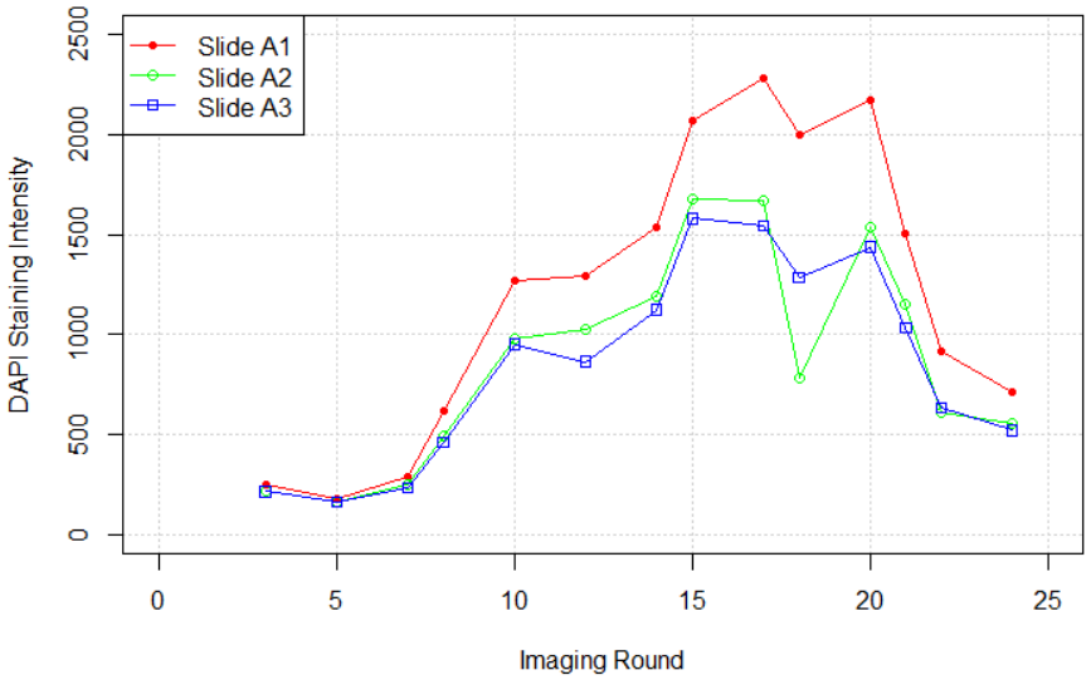

Supplementary Figure S1. Median DAPI Grid32 object intensity by DAPI imaging round and TMA slide.

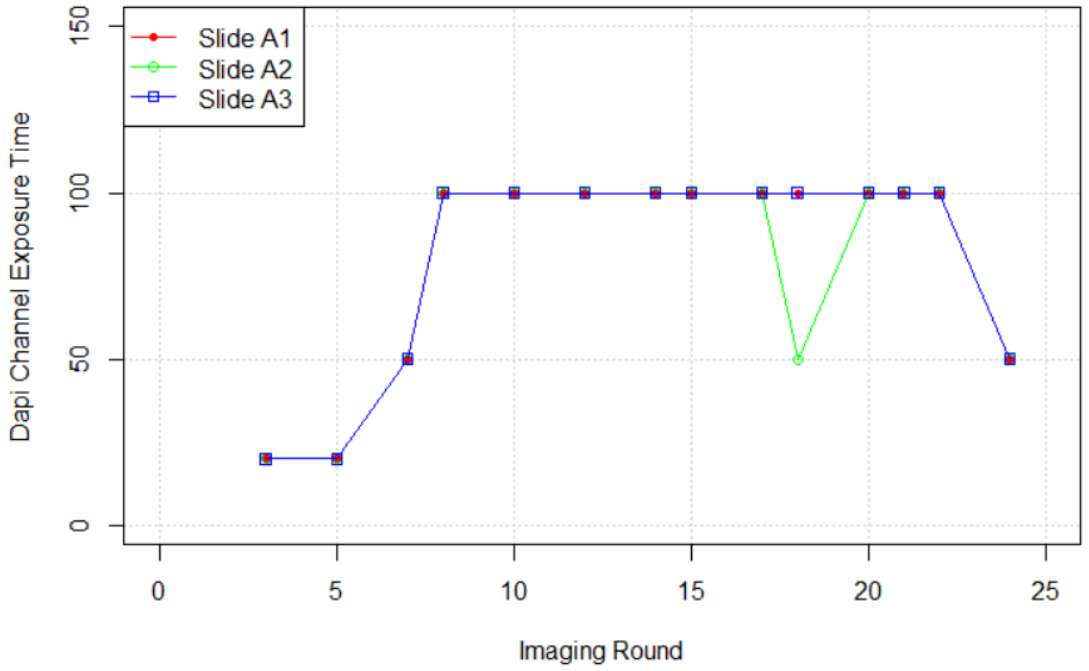

Supplementary Figure S2. DAPI Exposure time (milliseconds) by DAPI imaging round and TMA slide.

Normalization methods

As described in the main paper, we assembled a list of candidate normalization methods after performing a literature search. We specifically searched for methods that had been previously applied to bioimages as well as approaches used in transcriptomics. We filtered out approaches that required specific knowledge of the samples or sample layouts on the tissue slides. We did not consider any techniques that required training a model. For example, we did not include techniques that use specific segmented features from the bioimage for normalization. Such techniques can be powerful but tend to be less general. We were primarily interested in finding robust methods with broad application across tissue types and slide layouts. Finally, we limited our study to techniques that had been implemented in the R programming language (e.g. See https://www.bioconductor.org/). Given that we have released the data and R-scripts it should be possible for others in the future to evaluate and compare alternative techniques. We settled on a list of six methods listed in Table 1 of the main manuscript with details in Supplementary Table 3.

A slide is composed of one or more samples that undergoes a batched process of staining and imaging. If there are ten slides, then there are 10 batches that need to be normalized. We are focused on batch normalization and seek to remove any systematic experimental offsets that occurs between slides (i.e. batches). Each sample on a slide is imaged. Furthermore, the pixels within each image can be aggregated into objects (e.g. segmented cell objects, grid-based objects). The intensity of each object is the mean of pixel intensities within the object's boundaries. The objects may represent the pixels of the entire image such as with grid-based object workflow (Figure 1 of main manuscript) or a subset of pixels such as the segmented cell object workflow. In either case, it is possible to have different number of objects per slide. Some normalization techniques require having the same number of objects per batch (e.g. SQUA, MRN, TMM) while others do not (e.g. Median and Quantile such as Q50, Q75, UQUA). If the number of objects per batch is both not equal and small in number (<100) normalization will be less robust. However, in our studies the number of objects was very high (>100,000). To work with batches of equal number of objects, we randomly sampled a set of objects from each slide so that the number of objects that were sampled was equal to the number on the slide with the minimum number of objects. This sampling was performed in the R programing language with replacement flag set to false. In other words, the sampling function can only pick one unique object from a slide once. For slides with more objects than the minimum number objects, not every object might

be used. This may cause some hesitation until you evaluate the contribution that this contributes relative to the experimental offsets that are being corrected for.

Supplementary Table S3. Summary of normalization methods evaluated.

Method	Description	Method requires equal number of objects per batch to perform the normalization	Comparison with other methods
Median Normalization	The normalized intensity of object j found in image k is equal to the raw intensity of object j shifted by the differences in median intensity for all objects across all images minus the median intensity of all objects within image k $I_{k,j}^{norm} = I_{k,j}^{raw} + M_{all} - M_k$ Where M_k is median of the objects within slide k, and M_{all} is the median of all objects across all slides.	No	Method uses an additive function so shape of the distribution does not change. Applying the normalization is computationally fast once all median values are computed.
Quantile (Q50, Q75) and Upper Quantile (Bullard 2010)	Aligning the distribution's upper quantile by multiplying a factor $I_{k,j}^{norm} = I_{k,j}^{raw} * F_k$ The multiplicative factor is the ratio of the quantile of the objects from all slides (Q_{all}) divided by the quantile of the objects within slide k (Q_k): $F_k = Q_{all}/Q_k$. See Bioconductor R package: NOISeq	No	Method modifies the distribution in a linear fashion through a multiplication factor. Applying the normalization is computationally fast the targeted quantile values are computed. Note that Q75 is the same as UQUA.
Smooth Quantile (Hicks 2018)	Approach that aligning the quantile based on the assumption that the distribution shape should be the same. See Bioconductor R package: qsmooth	Yes	Method attempts to match the quantiles (i.e. shape of the distribution) across batches and thus can be sensitive to tail behaviours and inappropriate to slides that are not well balanced for sample types, tissue, cell density, shape, etc.
MRN (median ratio normalization) (Maza 2013)	$I_{k,j}^{scaled} = \frac{I_{k,j}^{raw}}{\frac{\sum_{k=1}^{N_s} I_{k,j}^{raw}}{N_s}}$ Where Ns is the number of slides and the scaling factor F_k is the median of the scaled objects (j = 1 to N) intensities for slide k: $F_k = \text{Median}(I_k^{scaled})$ $I_{k,j}^{norm} = I_{k,j}^{raw} / F_k$ See Bioconductor R package: fCI with details of the function call deseq.median.ratio.normalization detailed previously (Tang 2016).	Yes	Computationally more involved and involves a step of computing a scaling factor $I_{k,j}^{scaled}$. The median of the scaling factor for a particular batch is used as the multiplication factor (i.e. division by F_k). See Maza 2016 for details and differences between MRN and TMM methods.
TMM (trimmed mean of the M-values Robinson and Oshlack 2010, Tarazona 2011, 2015)	Scaling factor is weighted average of ratio compare to the reference column, but outliers are excluded in the calculation. Equations are too complex to display here. See Bioconductor R package: NOISeq with details and code for the function call tmm with settings of logratioTrim = 0.3, sumTrim = 0.05, doWeighting = TRUE	Yes	Very robust method and the computationally most involved of all the methods compared. See Maza 2016 for details and differences between MRN and TMM methods.

DAPI segmented nuclei objects to normalize and evaluate

The number of DAPI segmented nuclei objects used for normalization was 297,430 when no extra filtering was applied. The number of DAPI segmented nuclei objects used for evaluation were further filtered to eliminate objects that were of lower image quality. The DAPI round-to-round pixel correlation for the pixels contained within each segmented object was used to characterize the object's image quality. For more details on computing the QC correlation metrics see Bello 2008. Objects with pixel-to-pixel correlation less than 90% correlation across all 14 rounds of DAPI staining and imaging were filtered out. The number of DAPI segmented objects remaining and used for ground truth evaluation were 144,315.

Supplementary Table S4. Distribution of DAPI segmented nuclei object areas

Quantile	0%	1%	5%	10%	25%	50%	75%	90%	95%	99%	100%
Area (pixels^2)	62	64	73	85	123	203	320	471	593	908	14500

Grid-based objects to perform normalization

Grid objects were created by simply dividing up each image into regular squares of a given dimension. For example, a grid size of 16 has an object area of 225 pixels^2 which is like the area of an average DAPI segmented nuclei object (median DAPI segmented nuclei object area is 203 pixels^2). We did not evaluate grid sizes below 16 because the number of grid objects per slide became prohibitive with respect to computational time and memory. At 20x magnification a pixel width is ~0.39 microns. The Field of View (FOV) Image is 2560 x 2160 pixels^2 (998.4 x 842.4 microns^2) and the Grid Object Area = (grid size in pixels – 1) ^{2}.

Supplementary Table S5. Segmented grid object properties

Grid size (pixels)	**Grid size (microns)**	**Number of grid objects (per FOV image)**	**Number of grid objects (per FOV image width x height)**	**Grid object area (pixels^2)**	**Grid object area (microns^2)**
16	6.3	21,600	160 x 135	225	34.2
32	12.5	5,440	80 x 67.5	961	146
64	25	1,360	40 x 33.75	4.0×10^3	603
128	50	340	20 x 16.9	1.6×10^4	2.5×10^3
256	100	90	10 x 8.4	6.5×10^4	9.9×10^3
512	200	25	5 x 4.2	2.6×10^5	4.0×10^4
1024	400	9	2.5 x 2.1	1.0×10^6	1.6×10^5
2560	998.4	1	1 x 0.84	5.5×10^6	8.4×10^5

Test scenarios to evaluate normalization methods and workflows

Supplementary Table S6. Twenty-nine test scenarios.

Virtual Slides	Number of Slides	Exposure Time (ms) for each slide	Processing Time Interval between first and last slide (days)
RG003:RG005	2	20, 20	1.8
RG007:RG024	2	50, 50	33.4
RG008:RG010	2	100, 100	1.0
RG021:RG024	2	100, 50	15.8
RG003:RG020	2	20, 100	26.4
RG015:RG020	2	100, 100	4.9
RG008:RG020	2	100, 100	11.8
RG005:RG024	2	20, 50	41.4
RG012:RG015	2	100, 100	2.0
RG007:RG015	2	50, 100	11.8
RG003:RG015	2	20, 100	21.5
RG003:RG024	2	20, 50	43.1
RG008:RG017	2	100, 100	7.8
RG005:RG007:RG008	3	20, 50, 100	12.9
RG003:RG010:RG024	3	20, 100, 50	43.1
RG008:RG010:RG012	3	100, 100, 100	4.9
RG008:RG015:RG022	3	100, 100, 100	13.6
RG008:RG014:RG021	3	100, 100, 100	12.7
RG005:RG010:RG024	3	20, 100, 50	41.4
RG003:RG014:RG024	3	20, 100, 50	43.1
RG005:RG007:RG012	3	20, 50, 100	17.7
RG010:RG014:RG021	3	100, 100, 100	11.7
RG007:RG015:RG018	3	50, 100, 100	13.7
RG005:RG015:RG017	3	20, 100, 100	20.6
RG008:RG018:RG021	3	100, 100, 100	12.7
RG003:RG005:RG010	3	20, 20, 100	15.7
RG008:RG015:RG020	3	100, 100, 100	11.8
RG008:RG010:RG012:RG014:RG015:RG017:RG018:RG020:RG021:RG022	10	100, 100, 100, 100, 100, 100, 100, 100, 100, 100	13.6
RG003:RG005:RG007:RG008:RG010:RG012:RG014:RG015:RG017:RG018:RG020:RG021:RG022:RG024	14	20, 20, 50, 100, 100, 100, 100, 100, 100, 100, 100, 100, 100, 50	43.1

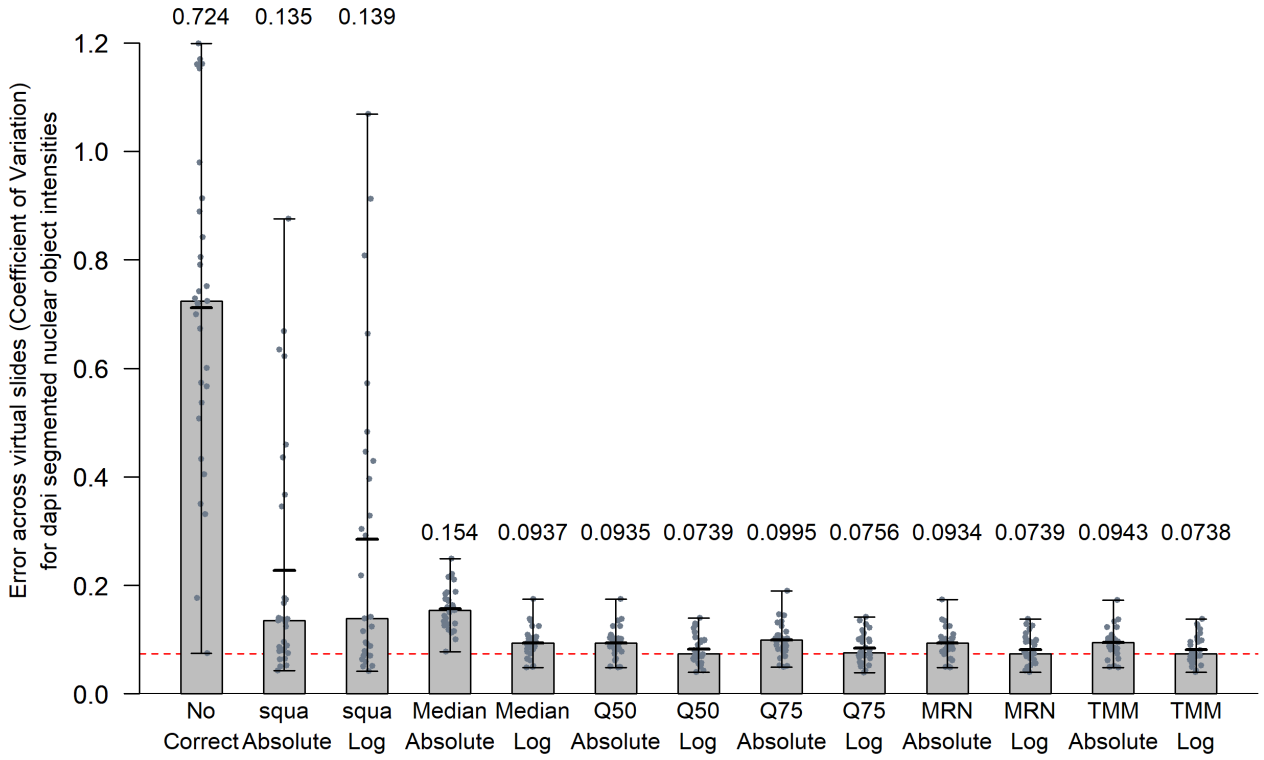

Supplementary Figure S3. Performance of normalization methods for DAPI segmented nuclei objects. The bar chart presents the performance of six normalization methods, applied in both absolute and log space, across 29 test scenarios relative to the uncorrected case (left most bar). The horizontal red line in the bar chart located at 0.0738 is achieved by the TMM method when applied in log space (right most bar). The height of each bar represents the median of the MEO-CVs across the 29-test scenarios. Within each bar there is a vertical line segment that represents the range in the 29 test values. The mean of the test cases is represented by a thicker horizontal line segment that is near the height of each bar.

Supplementary Table S7. Statistical testing the normalization methods for DAPI segmented nuclei objects. The table presents the p-values from the Wilcoxon rank sum test pairwise comparisons between conditions with Bonferroni corrections for multiple testing. The table presents the results of the six normalization methods, applied in both absolute and log space, across 29 test scenarios as well as the uncorrected case (left column of p-values). The data for each of these 13 conditions is plotted in supplementary figure S3.

		No	SQUA	MEDIAN	Q50	Q75	MRN	TMM	SQUA	MEDIAN	Q50	Q75	MRN
Method	**Space**	Corrrection	Absolute	Absolute	Absolute	Absolute	Absolute	Absolute	Log	Log	Log	Log	Log
SQUA	Absolute	1.7E-08											
MEDIAN	Absolute	2.6E-08	9.1E-01										
Q50	Absolute	1.7E-08	7.0E-02	1.7E-08									
Q75	Absolute	1.7E-08	1.9E-01	2.6E-08	2.6E-08								
MRN	Absolute	1.7E-08	6.2E-02	1.7E-08	7.0E-01	1.7E-08							
TMM	Absolute	1.7E-08	5.3E-02	1.7E-08	5.8E-02	2.4E-06	1.7E-01						
SQUA	Log	1.6E-06	1.0E-01	1.2E-01	3.8E-02	6.0E-02	3.8E-02	3.8E-02					
MEDIAN	Log	1.7E-08	7.3E-02	1.7E-08	5.5E-07	3.5E-08	7.0E-02	2.1E-01	3.8E-02				
Q50	Log	1.7E-08	1.7E-05	2.6E-08	5.8E-06	7.3E-08	4.6E-06	5.8E-06	6.8E-04	5.8E-06			
Q75	Log	1.7E-08	1.8E-04	2.6E-08	2.1E-03	3.4E-06	1.7E-03	2.0E-03	2.7E-03	1.8E-03	5.3E-06		
MRN	Log	1.7E-08	1.5E-05	1.7E-08	4.0E-06	5.4E-08	4.0E-06	5.3E-06	2.4E-04	4.0E-06	1.5E-02	3.5E-08	
TMM	Log	1.7E-08	1.5E-05	1.7E-08	4.0E-06	5.4E-08	3.9E-06	4.0E-06	2.4E-04	4.0E-06	6.9E-03	3.5E-08	9.3E-01

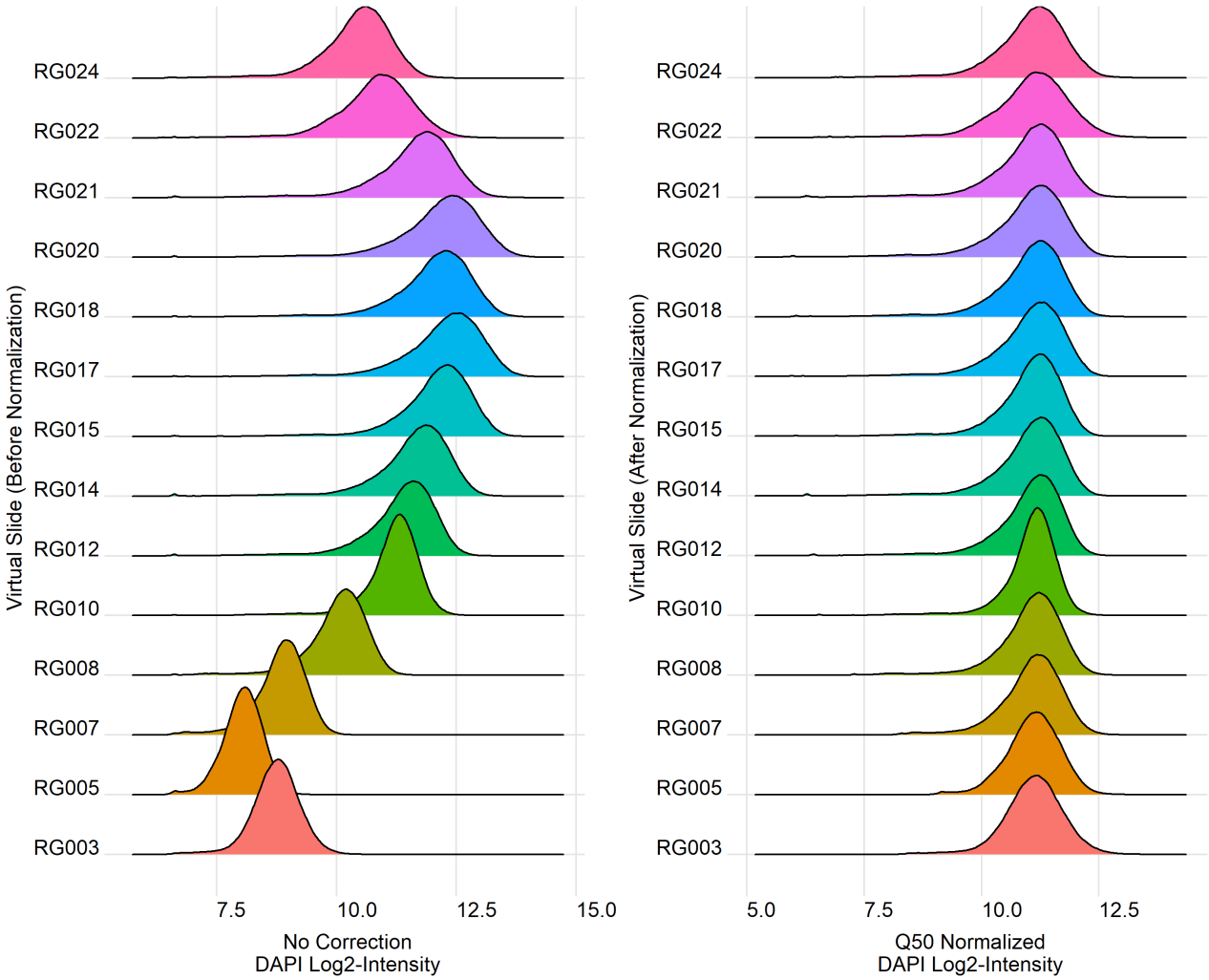

Supplementary Figure S4. Ridgeline plots of DAPI Log2-Intensities of segmented nuclei objects for each of the fourteen virtual slides before (No Correction plot on left) and after applying the 50% Quantile (Q50) normalization method in log space (right plot).

Figure S5B illustrates the small increase in the median of the MEO-CVs across the 29-test scenarios from 0.0738 obtained for no quality filtering to 0.0803 (9% reduction in performance) when applying the most stringent quality filtering tolerance.

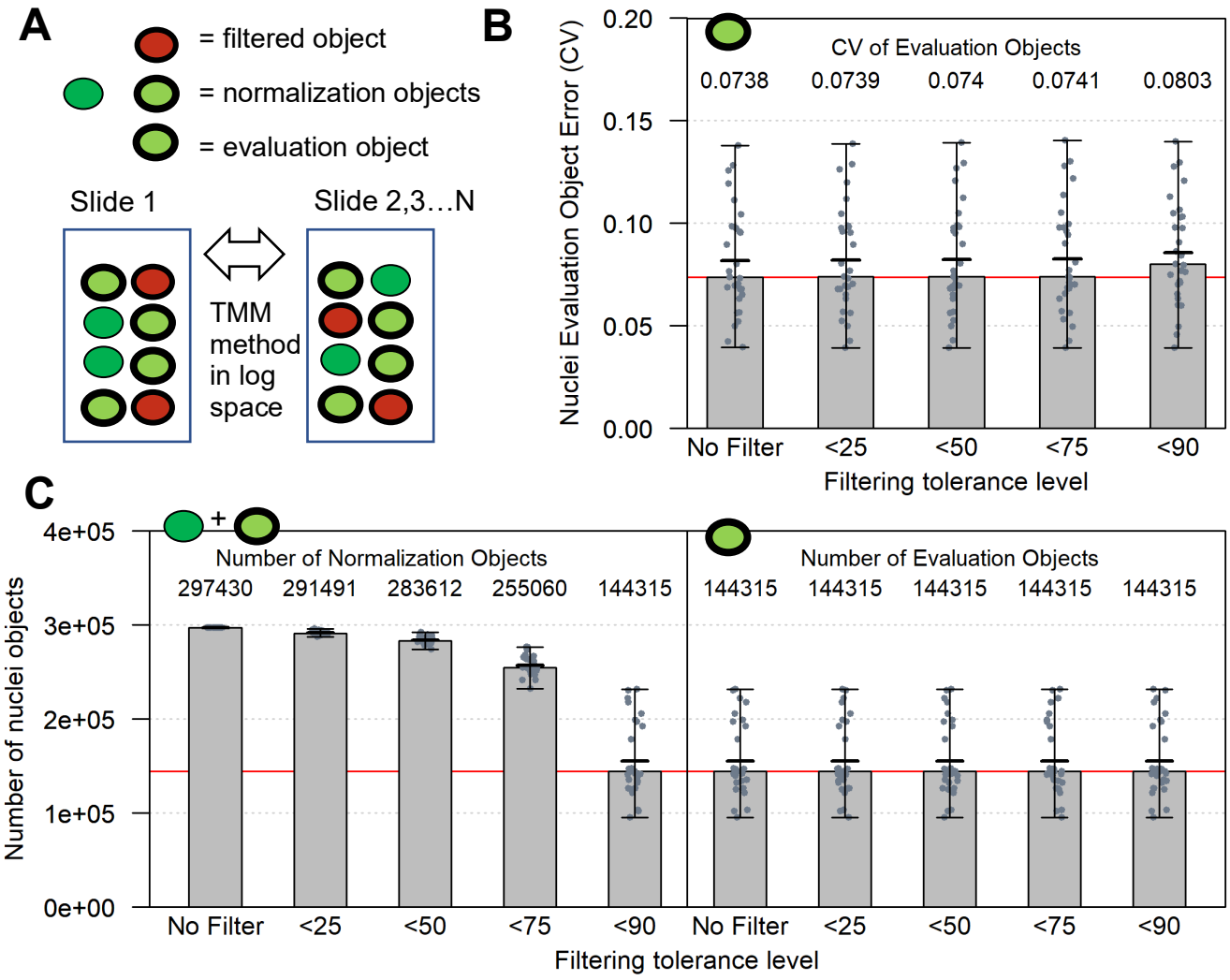

Supplementary Figure S5. Impact of filtering of objects for DAPI round-to-round correlation on performance of normalization. A) An object, and the aggregated pixels it represents, is filtered and not used to normalize the slide images (red oval) when its round-to-round pixel intensity correlation is less than the filtering tolerance level. An object is used to normalize but not used for evaluation (i.e. compute MEO-CVs) if its correlation is above the filtering tolerance but less than 90% (green oval). Finally, an object is used to normalize and evaluate when its correlation is above 90% (bold outlined green oval). B) The top bar chart shows that no-filtering of objects produced the lowest median of the MEO-CVs across the 29-test scenarios. The horizontal red line in the bar chart is located at 0.0738 achieved by the TMM method when applied in log space. C) The bottom bar chart presents the number of normalization objects (left side) and the number of evaluation objects (right side) for various object filtering tolerance levels.

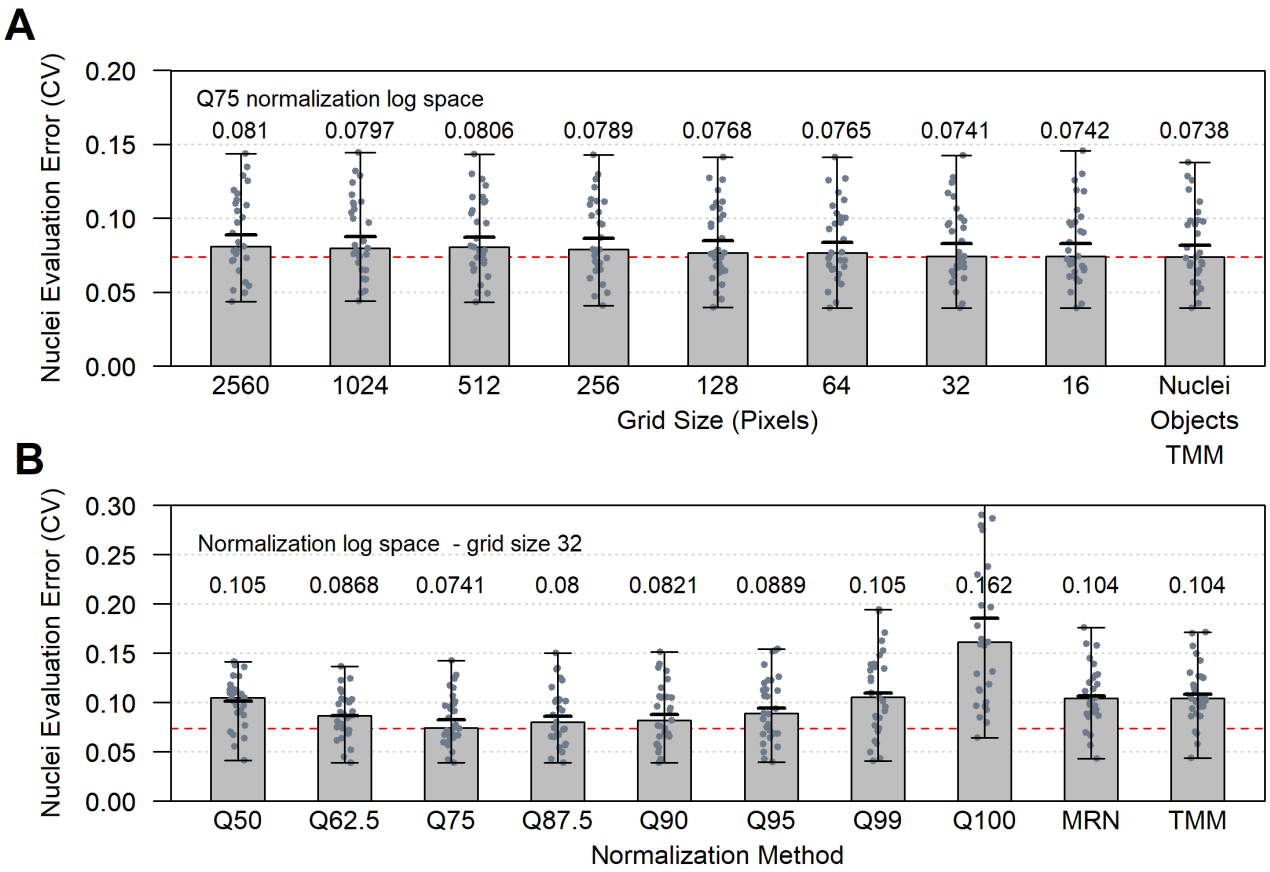

Supplementary Figure S6. Performance of normalization methods utilizing a grid-based approach. A) The top bar chart presents the performance using grids of various sizes. The 75% quantile (Q75) normalization method was applied in log space to Grid object intensities across 29-test scenarios. Each bar is for a different grid size that ranged from the entire image (2560 x 2160 pixels^2) down to a square grid size of 16 (15 x 15 pixels^2). A grid size of 16 is approximately equal to the median area of the nuclei segmented objects (203 pixels). The bar farthest to the right is a special case in which the TMM method has been applied in log space directly to the Segmented Nuclei objects. B) The bottom bar chart presents normalization methods applied in log space using a grid size of 32. Quantile normalization was applied using quantiles that ranged from 50% up to 100%. Performance of the MRN and TMM methods applied to the Grid objects (grid size = 32) are also presented. The horizontal red dashed line is located at 0.0738 in both bar charts.

Supplementary Table S8. Statistical testing the normalization methods for Grid-based objects using different grid sizes. The table presents the p-values from the Wilcoxon rank sum test pairwise comparisons between conditions with Bonferroni corrections for multiple testing. The table presents the results of 75% quantile (Q75) normalization to Grid objects with grid sizes that ranged from the entire image 2560 down to a grid size of 16. The performance of the TMM normalization method applied in log space directly to the Segmented Nuclei objects (i.e. entitlement) is also included.

	Grid16	Grid32	Grid64	Grid128	Grid256	Grid512	Grid1024	Grid2560
Grid32	6.2E-01							
Grid64	3.1E-01	2.2E-02						
Grid128	5.6E-02	4.1E-03	4.6E-04					
Grid256	6.6E-03	3.9E-04	5.4E-05	6.8E-06				
Grid512	1.5E-03	1.0E-04	1.2E-05	6.9E-06	9.3E-05			
Grid1024	1.7E-04	2.1E-05	1.1E-05	7.6E-05	4.3E-03	9.1E-02		
Grid2560	2.4E-04	3.3E-05	1.1E-05	7.1E-06	2.7E-05	8.6E-04	2.3E-02	
NucleiSCA TMM	7.7E-02	9.3E-02	2.0E-03	7.4E-04	6.8E-06	2.5E-06	9.4E-07	9.4E-07

Supplementary Table S9. Statistical testing the normalization methods Grid-based objects with a grid size of 32 using different quantiles for Quantile normalization. The table presents the p-values from the Wilcoxon rank sum test pairwise comparisons between conditions with Bonferroni corrections for multiple testing. The table presents the results of Quantile normalization to Grid objects (grid size = 32) for quantiles that ranged from 50% up to 100%. The performance of the MRN and TMM methods applied to the Grid objects is also shown for comparison purposes.

	Q50	Q62.5	Q75	Q87.5	Q90	Q95	Q99	Q100	MRN
Q62.5	1.2E-07								
Q75	7.6E-06	1.1E-02							
Q87.5	2.8E-03	8.0E-01	1.1E-02						
Q90	1.3E-02	7.5E-01	5.2E-03	4.4E-06					
Q95	2.4E-01	6.3E-02	3.3E-05	1.9E-06	3.2E-06				
Q99	3.5E-01	8.5E-04	1.8E-06	1.9E-06	1.9E-06	1.9E-06			
Q100	7.6E-06	1.2E-07	6.7E-08	6.7E-08	6.7E-08	6.1E-07	6.2E-05		
MRN	9.2E-02	6.7E-08	1.9E-06	2.6E-03	9.0E-03	1.7E-01	7.7E-01	6.0E-06	
TMM	1.0E-02	6.7E-08	5.2E-07	1.1E-03	5.9E-03	9.4E-02	9.5E-01	1.4E-05	3.7E-02

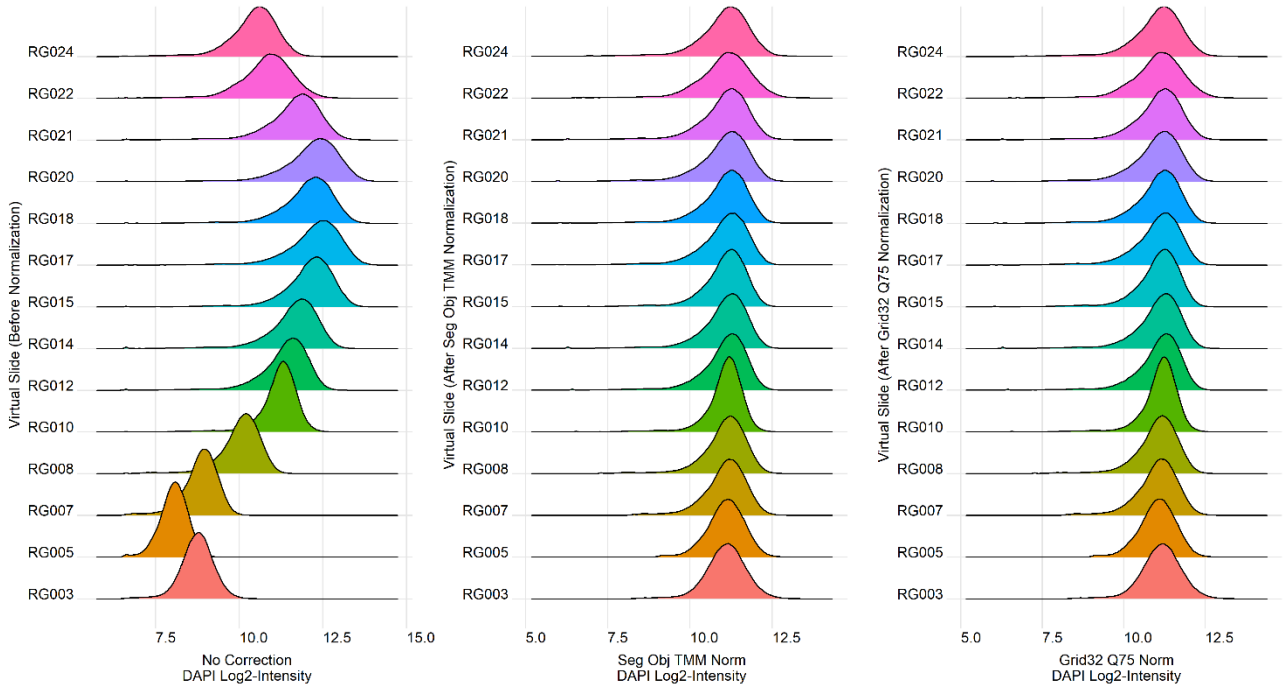

Supplementary Figure. S7. Ridgeline plots of DAPI Log2-Intensities of segmented nuclei objects for each of the fourteen virtual slides before (No Correction) normalization (left plot), and correcting the data by applying the TMM method directly to the segmented nuclei objects in log space (middle plot), and finally by normalizing the images first using Grid32 by the Q75 method in log space (right plot).

Supplementary Table S10. Effect of applying Grid-based normalization method to 24 antibody markers and DAPI across three physical TMA slides assessed by four control cell lines. The grid-based object normalization workflow with grids of 32 pixels in size and the Q75 method applied in log space was applied to three physical TMA slides. The normalization used measures from all samples including the patient tumor core samples (79) and the cell lines. The assessment was made on segmented cell objects from four cell lines HeLa, HCT116 XIAP-KO, MCF7, and JURKAT that were present throughout all staining rounds on all three TMA slides. The sums of squared difference (SSD) for the uncorrected and normalized cell line data are presented in along with the difference between the Normalized SSD minus the Uncorrected SSD (delta SSD). The cell line samples on the three physical slides were serial slices from the same cell line pellet and thus would be expected to have almost equivalent expression profiles across the three physical slides. Therefore, the expectation would be for the normalization method to reduce the SSD if there is a batch effect between the three slides. The mean change in SSD (Delta SSD) with normalization was -0.89 with a p-value = 0.08 for a one-sided paired sample t-test. The majority of the antibody markers did not appear to have a significant batch effect between slides from their histogram plots of the intensities prior to normalization.

Marker	Median Segmented Cell Object Log2 Intensity	SSD of Segmented Cell Objects after Grid Normalized	SSD of Segmented Cell Objects before Grid Normalized	Delta SSD
AE1	7.36	2.74	2.38	0.36
APAF1	9.66	0.65	1.32	-0.67
BAK	5.19	0.96	6.34	-5.38
BAX	7.55	0.17	1.71	-1.54
BCL2	8.04	0.43	1.54	-1.11
BCLXL	9.75	0.83	1.77	-0.94
CA9	9.79	2.20	0.94	1.26
CASP3	8.89	0.56	0.47	0.09
CASP9	9.45	0.91	1.06	-0.16
CD3	6.74	3.01	1.93	1.08
CD4	2.93	12.31	26.42	-14.11
CD45	6.34	0.17	0.20	-0.03
CD8	4.67	0.03	0.80	-0.78
DAPI	10.35	0.72	0.64	0.09
FOXP3	8.71	0.05	0.06	-0.02
GLUT1	8.16	0.40	0.24	0.16
HLA_I	9.13	0.15	0.01	0.14
KI67	10.40	0.45	0.09	0.36
MCL1	11.61	0.08	0.03	0.05
NAKATPASE	11.67	0.24	0.06	0.19
PCK26	11.98	0.40	0.07	0.33
PD1	12.49	0.34	0.09	0.25
S6	12.47	0.69	0.31	0.38
SMAC	12.16	0.96	4.13	-3.18
XIAP	12.37	1.25	0.46	0.79

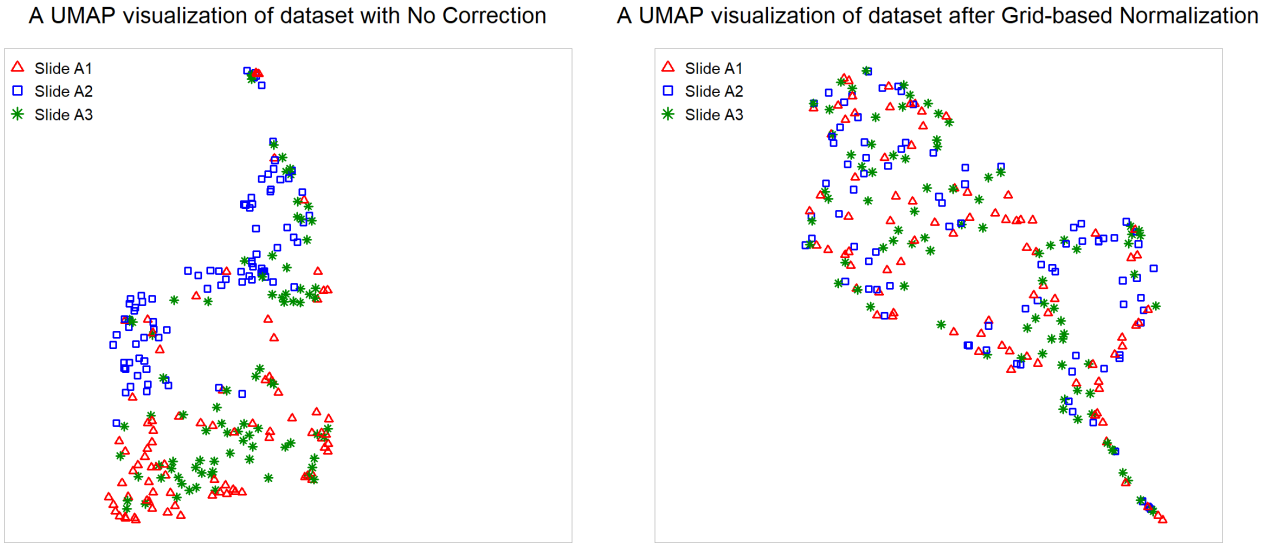

Supplementary Figure. S8. Uniform Manifold Approximation and Projection (UMAP) plots of the high-dimensional data before and after normalization. The data includes the twenty-four antibody markers as well as DAPI listed in supplementary table S10 for three slides with serial tissue slices. The UMAP plot on the left is the dataset prior to normalization (No Correction) and the UMAP plot on the right is after applying Grid-based normalization method using Grid32 and the Q75 method in log space. The batch effect in the three slides is indicated by the clustering of the blue squares, and red triangles observed in the plot om the left which is not observed after normalization for the plot on the right.